AN ACCURATE METHOD OF CALCULATING THE GRADIENTS OF SEISMIC WAVE REFLECTION COEFFICIENTS TO ROCK PROPERTIES IN TRANSVERSELY ISOTROPIC MEDIA

YIFEI BAO, JINGYI CHEN and XIAOBO LIU

Seismic Anisotropy Group, Department of Geosciences, The University of Tulsa, 800 South Tucker Drive, Tulsa, OK 74104, U.S.A. jingyi-chen@utulsa.edu

(Received February 11, 2019; revised version accepted February 29, 2020)

ABSTRACT

Bao, Y., Chen, J. and Liu, X.B., 2020. An accurate method of calculating the gradients of seismic wave reflection coefficients to rock properties in transversely isotropic media. *Journal of Seismic Exploration*, 29: 275-297.

The amplitude versus offset (AVO) inversion technique plays a critical role in exploration geophysics. The key issue of AVO inversion is the computational accuracy of the gradients of seismic wave reflection coefficients (SWRCs) to rock properties. Additionally, the anisotropic medium has the better representation of the earth than the isotropic medium. These issues will lead deviations in AVO process and weak the reliability of the final results. In this paper, we propose to develop a method of accurately calculating the gradients of SWRCs to rock properties (e.g., P- and S-velocities, density and anisotropic parameters) in transversely isotropic (TI) media. We calculate SWRCs in TI media by adding an anisotropic perturbation term on the exact Zoeppritz equations of the isotropic part. We obtain the partial derivatives of SWRCs to rock properties through a series of simple linear equations which not only keep a high accuracy but also offer a low computational cost. Finally, based on numerical tests, we plot the curves of SWRCs and partial derivatives of SWRCs with respect to rock properties and analyze their features.

KEY WORDS: exact Zoeppritz equations, accurate gradient solution, transversely isotropy.

0963-0651/20/$5.00

INTRODUCTION

Detecting or inferring the properties of subsurface structure by seismic data is an important procedure in oil/gas exploration (Sun and Zhao, 2006; Liu et al., 2012; Russell, 2014). The amplitude versus offset (AVO) inversion is a widely used method that can effectively estimate lithology and fluid properties through seismic data (Shuey, 1985; Rutherford and Williams, 1989; Hampson, 1991; Lu et al., 2018). Currently, most AVO inversions apply the approximate expressions of the Zoeppritz equations to generate seismic wave reflection coefficients (SWRCs) (Bortfeld, 1961; Mallick, 1995; Simmons and Backus, 1996; Wang, 1999; Li et al., 2005; Shou et al., 2006; Alemie and Sacchi, 2011; Zong et al., 2012; Lu et al., 2018). Compared with the exact Zoeppritz equations, these approximations are easier to calculate and can work well under the conditions of small incidence angle and weak-contrast reflection interface. While, with the increase of the complexity of reservoir structure, these conventional AVO methods are not suitable. It is hard to satisfy the requirement of the approximation like a weak-contrast interface in such an intricate structure. Therefore, the SWRCs calculated by the conventional AVO methods will be not accurate enough. Since a small error in the computation will lead to a large misfit by the accumulation during the iterative procedure of inversion. As a consequence, these inaccurate SWRCs may cause a large error for the final inversion results.

Additionally, in many AVO inversions, the medium is assumed to be isotropic (Aki and Richards, 1980; Shuey, 1985; Castagna and Backus, 1993; Tura and Lumey, 1999; Wang, 1999; Liu et al., 2012; Liu et al., 2019). However, as Thomsen (1986) indicates, most sedimentary rocks have weak anisotropy that can generate nonnegligible phenomena in exploration geophysics. Especially, the vertical transverse isotropy (VTI) is common in the earth crust (Backus, 1962; Thomsen, 1986; Carcione et al., 1991; Sidler and Holliger, 2010). Mallick and Frazer (1991), which has been proven that the P-wave reflection response from a VTI medium is azimuthally dependent. Tsvankin (1995) showed the important characteristic of the transversely isotropic (TI) directivity factor for the incident seismic wave in AVO inversion. Thus, previous isotropic AVO methods may make some big errors in the inversion results.

A significant amount of research has focused on calculating reflection coefficients in TI media. Banik (1987) presented that Thomsen anisotropic parameters can effectively describe AVO characteristics in the TI media.

A case study of AVO in VTI media for the different classes of gas sands has been found by Kim et al. (1992). Vavryčuk (1999) derived the approximate formulae for the reflection and transmission coefficients of PP and PS plane waves at weak-contrast interfaces in weakly anisotropic elastic media. However, all these studies are under the assumption of weak contrast, and use the approximate expressions of the Zoeppritz equations.

In AVO inversion, we often calculate gradients of SWRC to rock properties using finite-difference methods (Lu et al., 2018). However, it may lead to higher computational cost and instability. The purpose of this paper is to overcome these shortages of conventional AVO methods and develop a method of accurately calculating the gradients of SWRCs to rock properties (e.g., P- and S-velocities, density and anisotropic parameters) in TI media. The partial derivatives of SWRCs to rock properties can be obtained through a series of simple linear equations which not only keep a high accuracy but also offer a low computational cost. In addition, we apply the exact Zoeppritz equations to compute SWRCs in the isotropic part, and add an anisotropic perturbation term on the isotropic part to help us calculate SWRCs in the TI medium. Due to the huge computational cost of the exact Zoeppritz equations for TI media (Daley and Hron, 1977), we employ the Rüger's (2002) reflection coefficient equations for the VTI medium as the TI perturbation term. Rüger's equations include effective anisotropy parameters (known as Thomsen parameters) which can simply and precisely describe the influence of transversely isotropy on SWRCs (Booth et al., 2016). However, we should make it clear that our proposed method does not suffer any limitations for weak anisotropy and weak-contrast reflection interfaces.

Finally, we plot the curves of SWRCs in all three classes of AVO and compare them with conventional methods in TI media. The results show a significant improvement of our proposed method in computational cost and accuracy.

THEORY

In order to calculate seismic wave reflection coefficients (SWRCs) in anisotropic media, we add an anisotropic perturbation term on the isotropic part (Daley and Hron, 1977). It can be written as:

$$R = R_{iso} + R_{anis} \ , \tag{1}$$

where R_{iso} and R_{anis} denote the isotropic and anisotropic parts, respectively.

Therefore, the gradients of SWRCs with respect to rock properties are expressed as:

$$\frac{\partial R}{\partial m} = \frac{\partial R_{iso}}{\partial m} + \frac{\partial R_{anis}}{\partial m} \quad , \tag{2}$$

where the elements of parameter matrix m represent the values of P- and S-wave velocities, the density, and Thomsen parameters.

Isotropic media

Unlike using the approximate Zoeppritz equations in the isotropic part (Lu et al., 2018), we use the exact Zoeppritz equations to calculate SWRCs:

$$R_{iso} = A^{-1}B \quad , \tag{3}$$

where

$$A = \begin{pmatrix} \cos\alpha & -\sin\beta & \cos\alpha' & \sin\beta' \\ \sin\alpha & \cos\beta & -\sin\alpha' & \cos\beta' \\ \cos 2\beta & -\eta_1 \sin^2\beta & -\rho_{21}\eta_2 \cos 2\beta' & -\rho_{21}\eta_3 \sin 2\beta' \\ \eta_1^2 \sin 2\alpha & \eta_1 \cos 2\beta & \rho_{21}\dfrac{\eta_3^2}{\eta_2}\sin 2\alpha' & -\rho_{21}\eta_3 \cos 2\beta' \end{pmatrix}, \tag{4}$$

$$R_{iso} = \begin{pmatrix} R_{PP} & R_{PS} & T_{PP} & T_{PS} \end{pmatrix}^T \quad , \tag{5}$$

$$B = \begin{pmatrix} \cos\alpha & -\sin\alpha & -\cos 2\beta & \eta_1^2 \sin 2\alpha \end{pmatrix}^T \quad . \tag{6}$$

In the above equations, α indicates the incidence angle of P-wave, β is the reflection angle of S-wave, α' and β' denote refraction angles of P- and S-waves respectively. $\eta_1 = V_{s1}/V_{p1}$, $\eta_2 = V_{p2}/V_{p1}$, $\eta_3 = V_{s2}/V_{p1}$ and $\rho_{21} = \rho_2/\rho_1$. V_P and V_S are the P-and S-wave velocities, ρ is the density of the medium. We use subscripts "1" and "2" to distinguish the upper and lower layers (Fig. 1).

We partially differentiate the equations of SWRCs with the parameter matrix m_{iso}, which includes the η_1, η_2, η_3 and ρ_{21}. The derivative equations can be written as:

$$A\frac{\partial R_{iso}}{\partial m_{\mathrm{iso}}} = -\frac{\partial A}{\partial m_{iso}} R_{iso} + \frac{\partial B}{\partial m_{iso}} \quad . \tag{7}$$

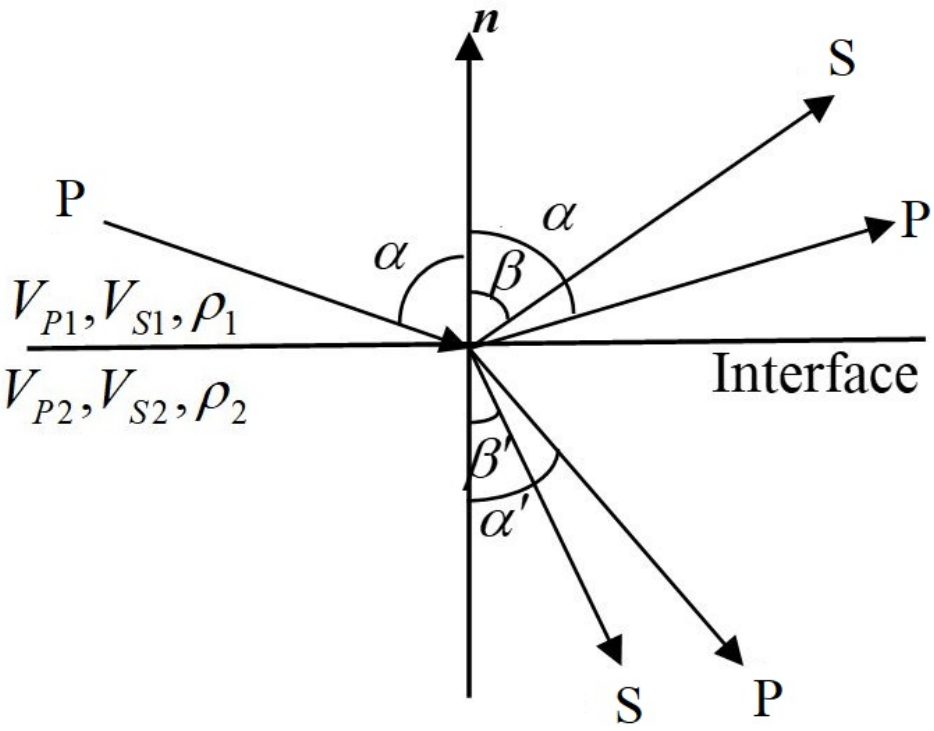

Fig. 1. Reflection and transmission of only P-wave incidence at an interface between two elastic media (Revised from Liu et al., 2019). n is the normal direction.

Based on eq. (4), we can calculate the partial derivatives of the reflection coefficients by obtaining the partial derivative equations of matrices $\boldsymbol{A}$ and $\boldsymbol{B}$. Further, by utilizing the chain rule of derivatives, we can easily compute the accurate partial derivative equations of SWRCs with respect to P- and S-velocities and density (Appendix A).

Transversely Isotropic (TI) media

Here, we apply the Rüger's reflection coefficient equations (Rüger, 2002) to calculate the PP and PS reflection coefficients in the vertical transverse isotropic (VTI) medium, which can be written as:

$$\begin{cases} R_{PP}^{anis} = \dfrac{1}{2}(\delta_2 - \delta_1)\sin^2\alpha + \dfrac{1}{2}(\varepsilon_2 - \varepsilon_1)\sin^2\alpha\tan^2\alpha \\ R_{PS}^{anis} = \left[\left(\dfrac{V_P^2}{2(V_P^2 - V_S^2)\cos\beta} - \dfrac{V_P V_S\cos\alpha}{2(V_P^2 - V_S^2)}\right)(\delta_2 - \delta_1)\right]\sin\alpha \\ \qquad + \left[\dfrac{V_P V_S\cos\alpha}{(V_P^2 - V_S^2)}(\delta_2 - \delta_1 + \varepsilon_1 - \varepsilon_2)\right]\sin^3\alpha \\ \qquad - \left[\dfrac{V_P^2}{(V_P^2 - V_S^2)\cos\beta}(\delta_2 - \delta_1 + \varepsilon_1 - \varepsilon_2)\right]\sin^3\alpha \\ \qquad + \left[\dfrac{V_S^2}{2(V_P^2 - V_S^2)\cos\beta}(\delta_2 - \delta_1)\right]\sin^3\alpha \\ \qquad + \left[\dfrac{V_S^2}{(V_P^2 - V_S^2)\cos\beta}(\delta_2 - \delta_1 + \varepsilon_1 - \varepsilon_2)\right]\sin^5\alpha \end{cases} \tag{8}$$

where ε and δ are known as Thomsen anisotropic parameters. The V_P and V_S is the vertical (symmetry-axis) velocities of the P- and S-waves, respectively:

$$\begin{cases} V_P = \dfrac{1}{2}\left(V_{P1} + V_{P2}\right) \\ V_S = \dfrac{1}{2}\left(V_{S1} + V_{S2}\right) \end{cases}. \tag{9}$$

The partial derivatives of the reflection coefficients with vertical velocities and Thomsen anisotropic parameters can be found in Appendix B.

NUMERICAL EXAMPLES

We first compare our new SWRCs with those generated by approximations of Aki and Richards (1980) and Shuey (1985) in the isotropic part to examine the effectiveness of our method. Based on the isotropic part, we add the anisotropic perturbation to figure out the difference between isotropic and anisotropic terms. Finally, we plot gradient curves of SWRCs with respect to rock properties to better understand the features of the partial derivatives of SWRCs.

Isotropic part

Here, we choose a class II model (isotropic part in Table 1), where the reflection interface represents an interface between mudstone and saturated-gas sandstone. Fig. 2 shows the comparison of reflection coefficients R_{PP} (the incident and reflected waves are both P-waves, incident angle range is $0^o - 40^o$) calculated by the exact, the Shuey's approximate (Shuey, 1985) and Aki and Richards' approximate (Aki and Richards, 1980) Zoeppritz equations in the class II AVO model, respectively. There is a clear split between the three curves. When incidence angle is small, the values of those reflection coefficients R_{PP} are almost same. With the incidence angle increasing, the difference between them becomes larger. This phenomenon verifies that the conventional approximate methods are suitable for small incident angle and our new method can improve the accuracy with the large incidence angle.

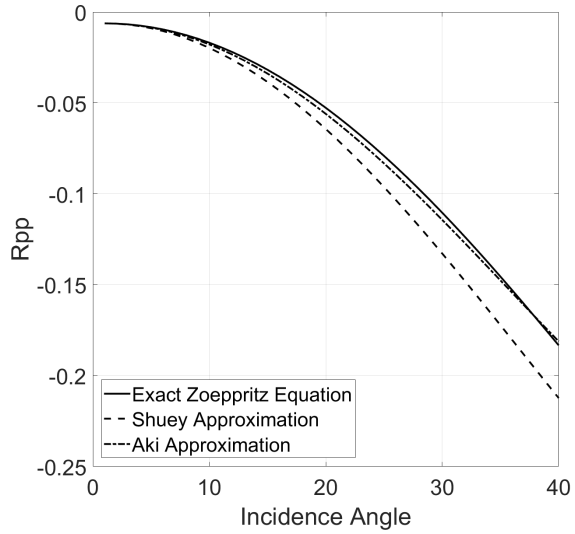

Fig. 2. The comparison of reflection coefficients R_{PP} by applying the exact, Shuey's approximate and Aki-Richards' approximate Zoeppritz equations in an isotropic medium (class II), respectively.

Table 1. Rock properties for the two-layer anisotropic model (class II). (Liu et al., 2012).

	V_P(m/s)	V_S(m/s)	ρ(g/cm^3)	δ	ε
Mudstone	1910	800	2.25	0.1	0.2
Saturated-gas sandstone	2202	1369	2.3	0.08	0.15

Table 2. Rock properties for the two-layer isotropic model (class I). (Castagna et al. 1998).

	V_P(m/s)	V_S(m/s)	ρ(g/cm^3)
Tight unit	3250	1780	2.44
Shale	2900	1330	2.99

Table 3. Rock properties for the two-layer isotropic model (class III). (Castagna et al. 1998).

	V_P(m/s)	V_S(m/s)	ρ(g/cm^3)
Shale	2590	1060	2.21
Gas sandstone	1650	1090	2.07

To further illustrate the significance of the exact Zoeppritz equations, we also plot the SWRCs curves for class I (Table 2) and class III (Table 3) of AVO models which are shown in Figs. 3 and 4, respectively. Figs. 3 and 4 show the same observations as Fig. 2 does. Those studies indicate that we can improve the accuracy of AVO inversion using the exact Zoeppritz equations.

Fig. 3. The comparison of reflection coefficients R_{PP} by applying the exact, Shuey's approximate and Aki-Richards' approximate Zoeppritz equations in class I model (Castagna et al. 1998), respectively.

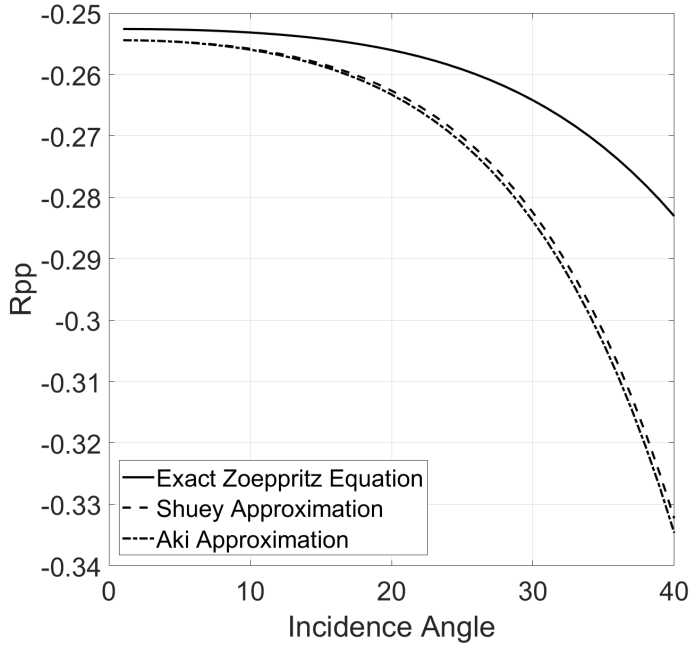

Fig. 4. The comparison of reflection coefficients R_{PP} by applying the exact, Shuey's approximate and Aki-Richards' approximate Zoeppritz equations in class III model (Castagna et al. 1998), respectively.

Anisotropic perturbation

We first take class II model (Table 1) as an example for the study in anisotropic media. As Fig. 5 indicates, the anisotropic perturbation term can generate a remarkable variation for reflection coefficients. The difference of reflection coefficients increases with the incident angle increasing. It proves the importance of the anisotropy for the SWRC's computation.

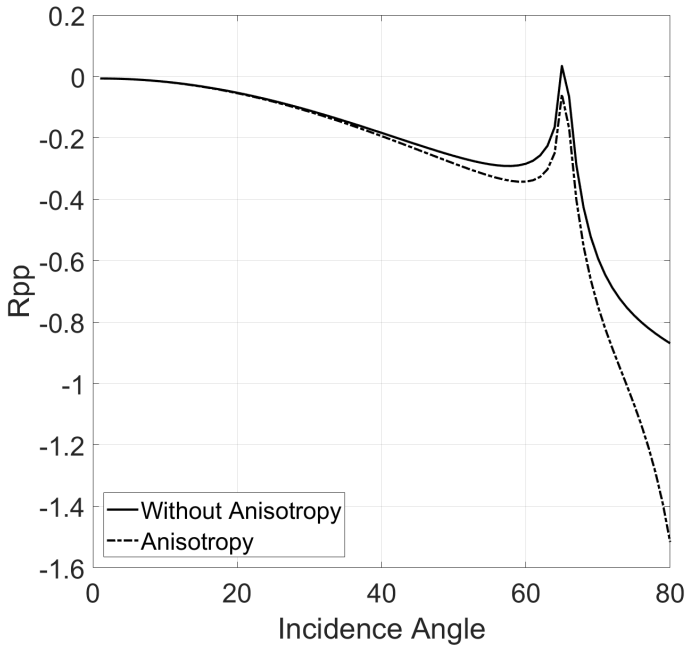

Fig. 5. The comparison of reflection coefficients R_{PP} with and without anisotropic perturbation term, respectively.

In order to further understand the influences of P- and S-velocities, densities and Thomsen anisotropic parameters to the SWRCs, we calculate the partial derivatives of the SWRCs with respect to the V_P, V_S, ρ, δ and ε, respectively. We will use the same incidence angle range $(0^o - 90^o)$ in the following studies. The results are shown in Figs. 6 to 13, where the incident wave is P-wave.

We first plot the partial derivatives of reflection coefficients R_{PP} with respect to V_{P1} and V_{P2} (Fig. 6). The real part of the partial derivatives of the R_{PP} with respect to V_{P1} and V_{P2} are shown in Fig. 6a. For real part of V_{P1}, there is a singular point at the critical angle. The partial derivative is increasing slowly with small incident angle increasing. As the incident angle close to the critical angle, the amplitude of reflection coefficients performs

exponential growth and back to zero when the incident angle is far away from the critical angle. Fig. 6b shows the imaginary part of the partial derivatives. The partial derivative of V_{P1} is zero before the critical angle and there is a large jump when the incident angle reach to the critical angle. After this jump, the partial derivative rapidly returns to zero. This discontinuity lets the partial derivatives become complex numbers, which means the phase shift generates. The real and imaginary parts of partial derivatives of V_{P2} are converse to the V_{P1}. As shown in Fig. 6, the computational instability will be caused around the critical angle due to the pike occurring at the critical angle ($\sim 65^{o}$). We should avoid using the seismic reflection data near the critical angle when carrying out seismic AVO inversion.

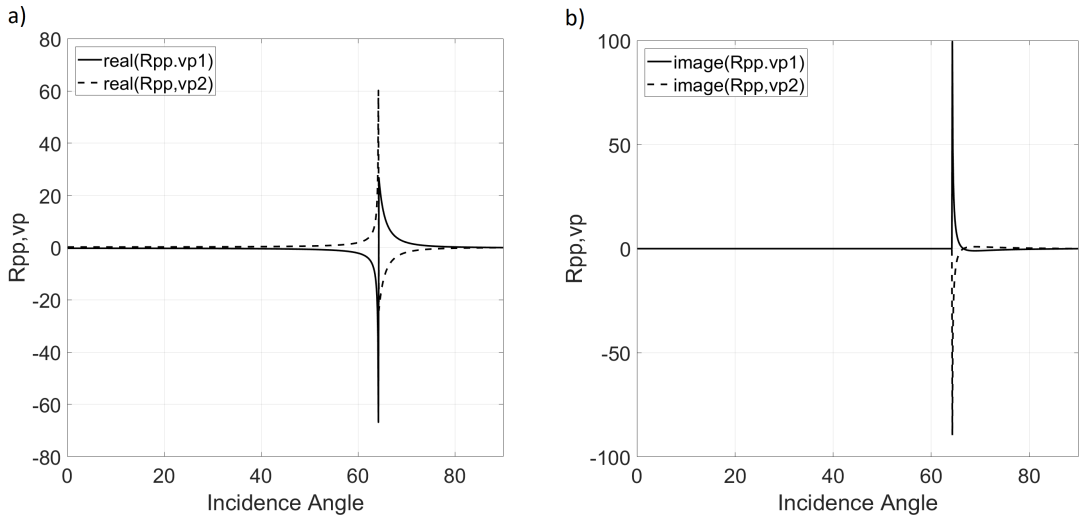

Fig. 6. The real (a) and imaginary (b) parts of partial derivatives of reflection coefficient R_{PP} with respect to V_{P1} and V_{P2} in the incidence angle range $0^{o} - 90^{o}$, respectively.

The real and imaginary parts of the partial derivative curves of R_{PP} with respect to V_{S1} and V_{S2} are shown in Figs. 7a and 7b, respectively. There is also a singular point at the critical angle. The real part of partial derivative with respect to V_{S1} increases with the incident angle increases (Fig. 7a). Upon the incident angle larger than the critical angle, the derivative starts to decrease when the incident angle increases. For imaginary part (Fig. 7b), the derivative is zero before the critical angle and decreases to zero after the pike. The curve regarding the V_{S2} is opposite of V_{S1} which has a larger amplitude. Comparing with Fig. 6, the curves of Fig. 7 are gentler, especially near the critical angle.

The partial derivatives of R_{PP} with respect to the densities are shown in Fig. 8. The trend of the curve regarding ρ_1 is similar as the derivative of V_{P1} that has a large jump near the critical angle and a singular point can be found on it. The polarities will change beyond the critical angle. And the derivative of R_{PP} with respect to ρ_2 shows the antipode of ρ_1. However, we notice that the real part of derivative curve of R_{PP} has a zero point within the range of critical angle.

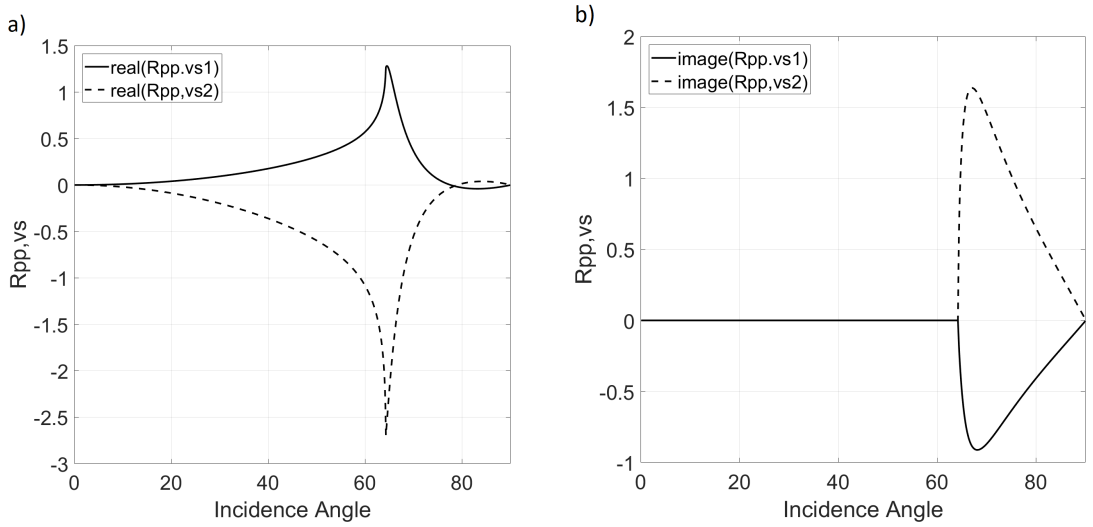

Fig. 7. The real (a) and imaginary (b) parts of partial derivatives of reflection coefficient R_{PP} with respect to V_{S1} and V_{S2}, respectively.

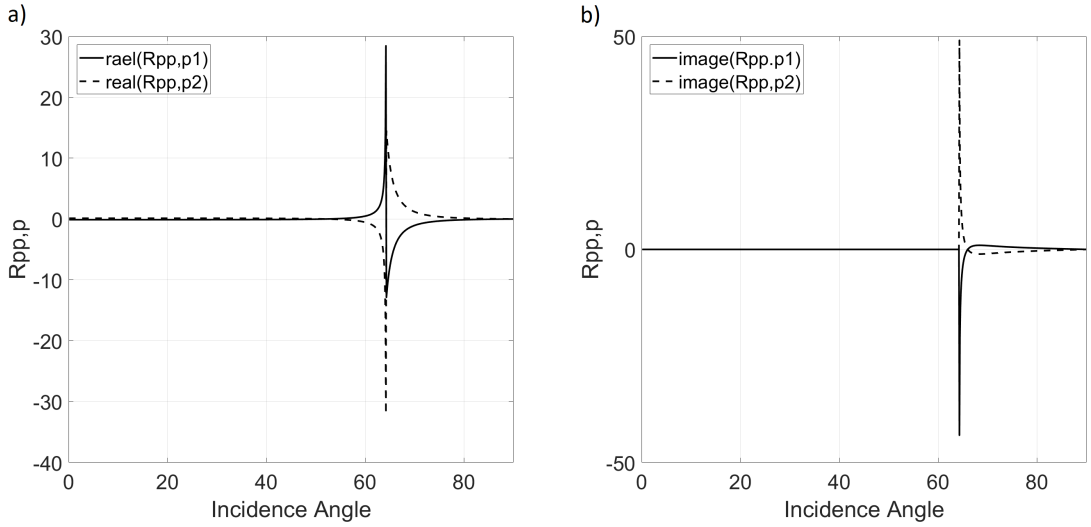

Fig. 8. The real (a) and imaginary (b) parts of partial derivatives of reflection coefficient R_{PP} with respect to ρ_1 and ρ_2, respectively.

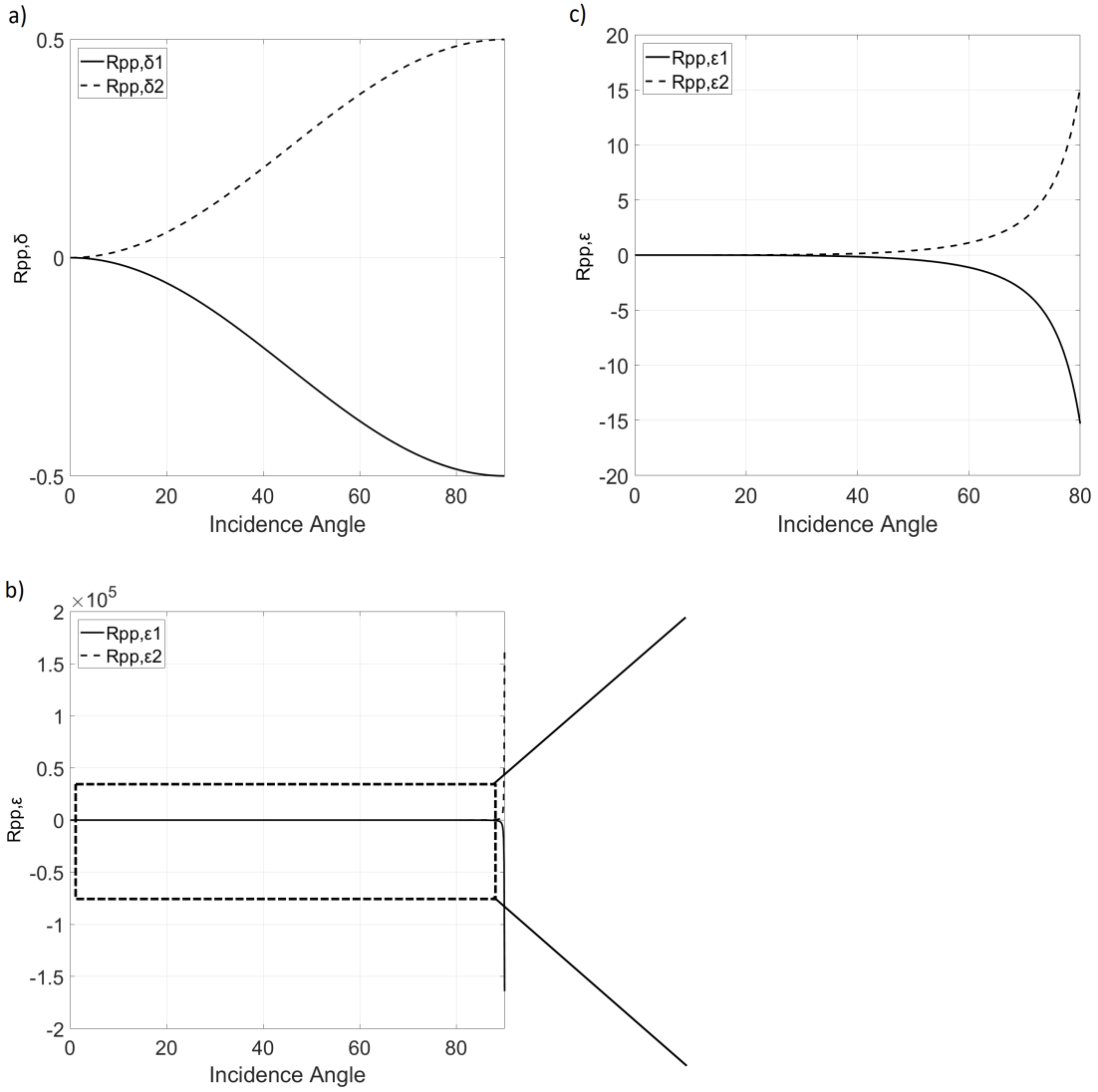

Fig. 9. The partial derivatives of reflection coefficient R_{PP} with respect to Thomsen parameters. (a): δ_1 and δ_2; (b): ε_1 and ε_2; (c): Zoom-in view of (b).

In Fig. 9, we plot the partial derivatives of R_{PP} with respect to Thomsen parameters. The partial derivative value of R_{PP} with respect to δ_1 increases with the increase of incidence angle (Fig. 9a). However, the partial derivative value of R_{PP} with respect to ε_1 is not sensitive in the range of small incidence angle (Fig. 9b). As the incidence angle is large enough, the derivative value of R_{PP} with respect to ε_1 becomes exponential growth with the increase of incidence angle increase. The partial derivative curve of R_{PP} with respect to δ_2 and ε_2 is reverse to δ_1 and ε_1, respectively.

We also show the partial derivative curves of R_{PS} (the incident wave is P-wave and reflected wave is S-wave) with respect to P-wave velocities, S-wave velocities, densities and Thomsen parameters in Figs. 10,11,12 and 13.

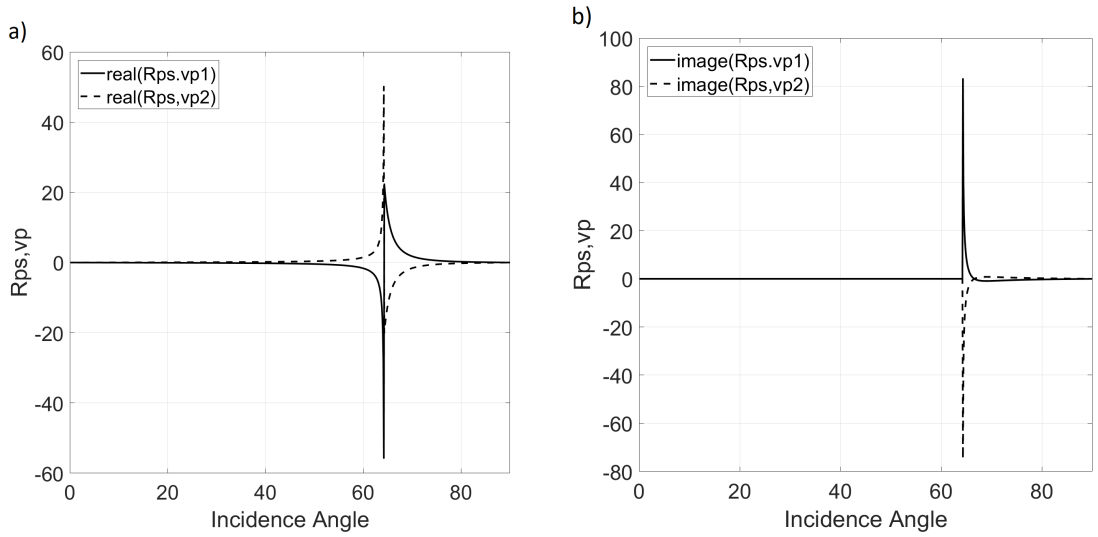

Fig. 10. The real (a) and imaginary (b) parts of partial derivatives of reflection coefficient R_{PS} with respect to V_{P1} and V_{P2}, respectively.

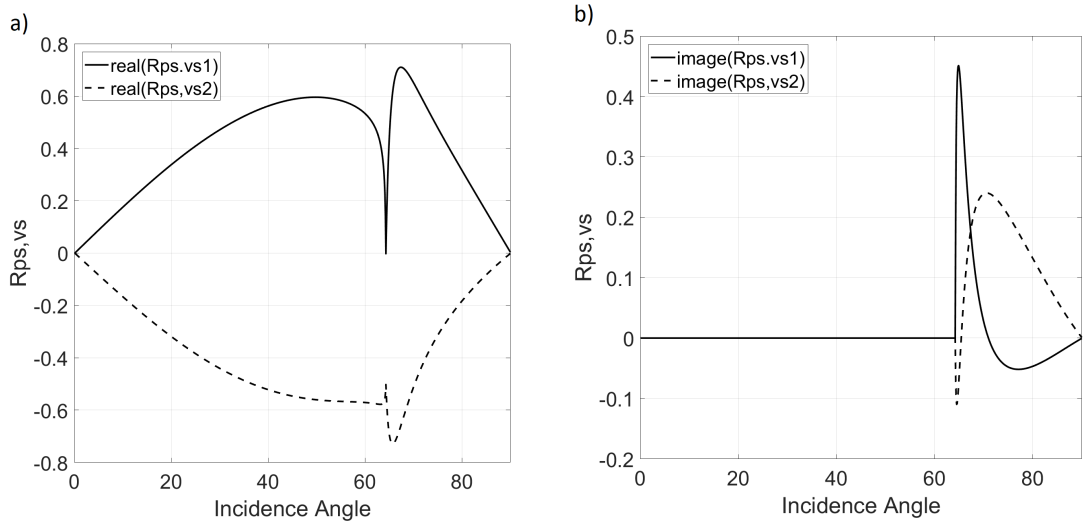

Fig. 11. The real (a) and imaginary (b) parts of partial derivatives of reflection coefficient R_{PS} with respect to V_{S1} and V_{S2}, respectively.

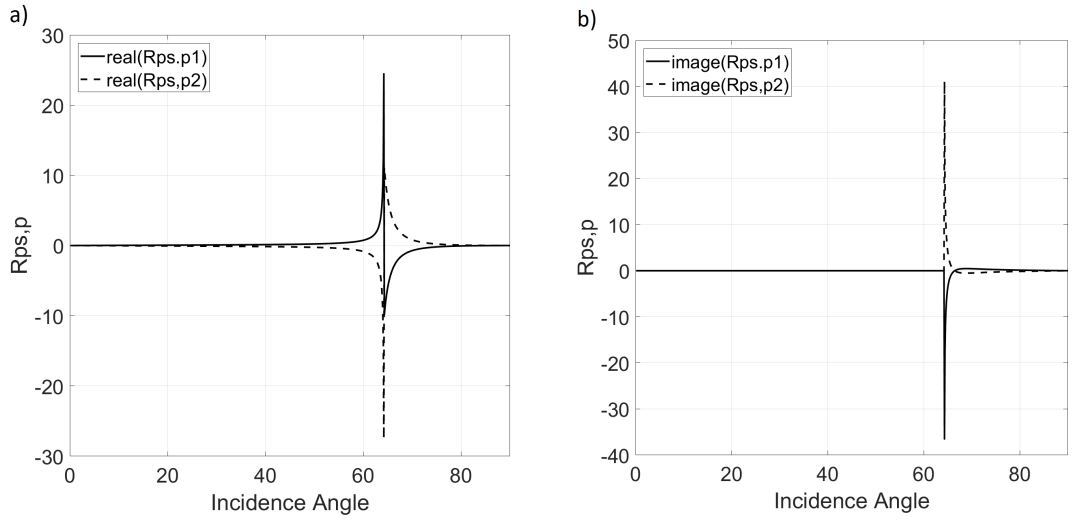

Fig. 12. The real (a) and imaginary (b) parts of partial derivatives of reflection coefficient R_{PS} with respect to ρ_1 and ρ_2, respectively.

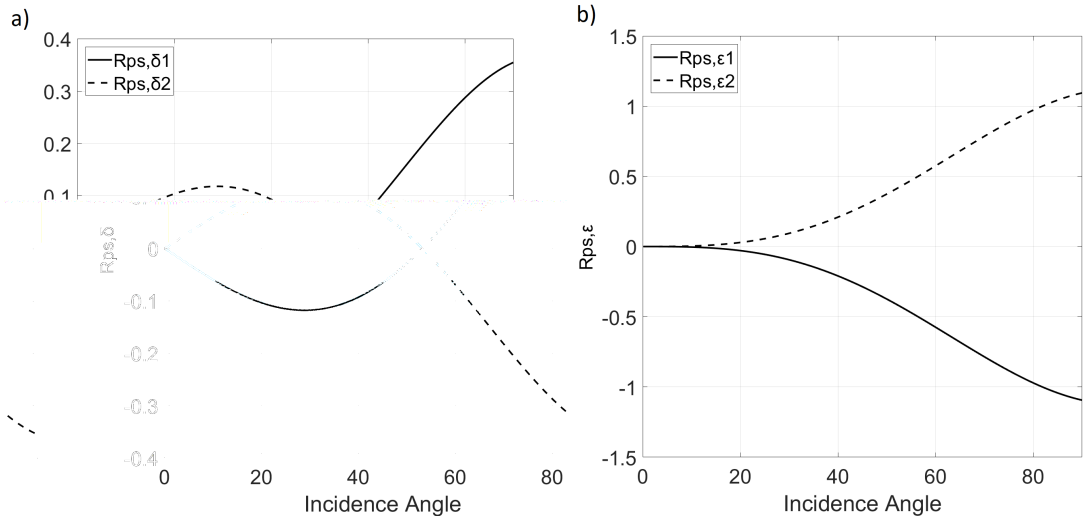

Fig. 13. The partial derivatives of reflection coefficient R_{PS} with respect to Thomsen parameters. (a): δ_1 and δ_2; (b): ε_1 and ε_2.

Readers can analyze the features of partial derivatives of R_{PS} as we do in the case of R_{PP}. Our studies here can not only help us better understand features of reflection coefficients, but also help us avoid the singular point when implementing AVO inversion.

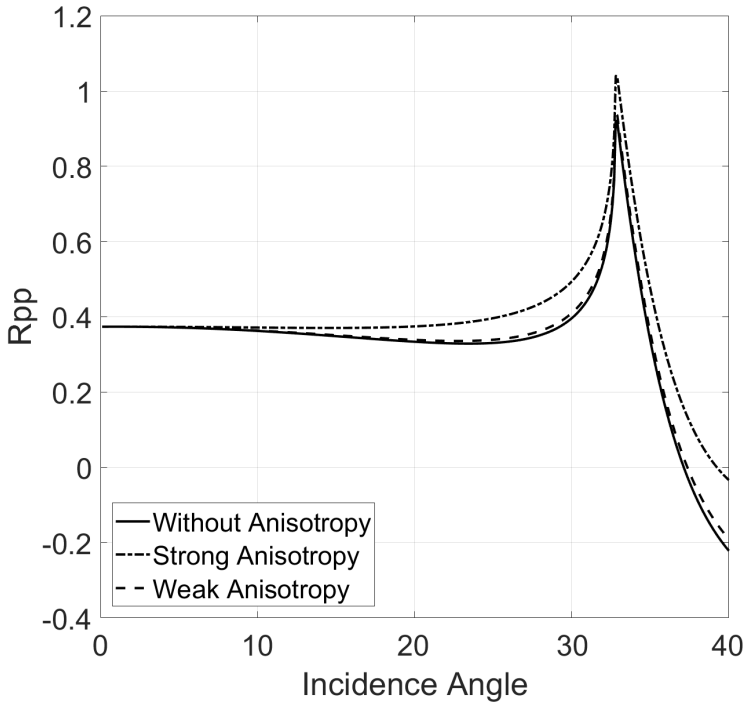

Fig. 14. The comparison of reflection coefficients R_{PP} with weak (~10%) and strong (~30%) anisotropy.

Table 4. Rock properties for the weak and strong anisotropic media in the bottom layer, respectively. (Thomsen, 1986).

	V_P(m/s)	V_S(m/s)	ρ(g/cm^3)	δ	ε
Mudstone (Top)	1910	800	2.25	0.1	0.2
Shale (Bottom,Weak~10%)	3794	2074	2.56	0.08	0.11
Shale (Bottom,Strong~30%)	3794	2074	2. 56	0.43	0.32

To further study anisotropic influence, we choose two more models (Table 4), which consist of two layers, respectively. The top layers are represented by the same mudstone in two models. The bottom layers are

represented by the shale with 10% and 30% anisotropy, respectively. The reflection coefficients R_{PP} are shown in Fig. 14. We can observe that the stronger the anisotropy the larger the difference of reflection coefficients calculated between the isotropic and anisotropic media. It also indicates that our method can work well in both weak and strong anisotropic media.

CONCLUSIONS

In this paper, we successfully calculated seismic wave reflection coefficients (SWRCs) in the transversely isotropic (TI) medium and improved the computational accuracy of the reflection coefficients. The numerical test demonstrated that the errors between the accurate solution and approximations cannot be ignored. We also established the partial derivative equations of the reflection coefficients to rock properties and reveal their characteristics. In addition, based on our accurate computational method, the gradients of SWRCs in an anisotropic medium can be obtained easily and speedily, which, consequently, can lead to a fast and precise AVO inversion.

ACKNOWLEDGEMENTS

The authors thank the anonymous reviewer for constructive comments and suggestions which greatly improve the quality of our paper.

REFERENCES

Aki, K. and Richards, P., 1980. Quantitative Seismology - Theory and Method. W.H. Freeman and Co., San Francisco.

Alemie, W. and Sacchi, M.D., 2011. High-resolution three-term AVO inversion by means of a Trivariate Cauchy probability distribution. Geophysics, 76(3): R43-R55.

Backus, G.E., 1962. Long-wave elastic anisotropy produced by horizontal layering. J. Geophys. Res., 67: 4427-4440.

Banik, N.C., 1987. An effective anisotropy parameter in transversely isotropic media. Geophysics, 52: 1654-1664.

Booth, A.D., Emir, E. and Diez, A., 2015. Approximations to seismic AVA responses: Validity and potential in glaciological applications. Geophysics, 81(1), WA1-WA11.

Bortfeld, R., 1961. Approximations to the reflection and transmission coefficients of plane longitudinal and transverse waves. Geophys. Prosp., 9: 485-502.

Carcione, J.M., Kosloff, D. and Behle, A., 1991. Long-wave anisotropy in stratified media: A numerical test. Geophysics, 56: 245-254.

Castagna, J.P. and Backus, M.M., 1993. Offset-dependent Reflectivity - Theory and Practice of AVO Analysis. SEG, Tulsa, OK.

Castagna, J.P., Swan, H.W. and Foster, D.J., 1998. Framework for AVO gradient and intercept interpretation. Geophysics, 63: 948-956.

Daley, P.F. and Hron, F., 1977. Reflection and transmission coefficients for transversely isotropic media. Bull. Seismol. Soc. Am., 67: 661-675.

Hampson, D., 1991. AVO inversion, theory and practice. The Leading Edge, 10(6), 39-42.

Li, H., 2005. The application of wide-angle reflection method in central Tarim basin. Geophys. Prosp. Petrol. (in Chinese), 44: 292-295.

Kim, K.Y., Wrolstad, K.H. and Aminzadeh, F., 1993. Effects of transverse isotropy on P-wave AVO for gas sands. Geophysics, 58: 883-888.

Liu, X., Chen, J., Liu, F., Wang, A. and Zhao, Z., 2019. Accurate Jacobian matrix using the exact Zoeppritz equations and effects on the inversion of reservoir properties in porous media. Pure Appl. Geophys., 176: 315-333.

Liu, X., Liu, F., Meng, X. and Xiao, J., 2012. An accurate method of computing the gradient of seismic wave reflection coefficients (SWRCs) for the inversion of stratum parameters. Surv. Geophys., 33: 293-309.

Lu, J., Wang, Y., Chen, J. and An, Y., 2018. Joint anisotropic amplitude variation with offset inversion of PP and PS seismic data. Geophysics, 83(2), N31-N50.

Mallick, S., 1995. Model-based inversion of amplitude-variations-with-offset data using a genetic algorithm. Geophysics, 60: 939-954.

Mallick, S. and Frazer, L.N., 1991. Reflection/transmission coefficients and azimuthal anisotropy in marine seismic studies. Geophys. J. Internat., 105: 241-252.

Rüger, A., 2002. Reflection Coefficients and Azimuthal AVO Analysis in Anisotropic Media. SEG, Tulsa, OK.

Russell, B.H., 2014. Prestack seismic amplitude analysis: An integrated overview. Interpretation, 2(2), SC19-SC36.

Rutherford, S.R. and Williams, R.H., 1989. Amplitude-versus-offset variations in gas sands. Geophysics, 54: 680-688.

Shou, H., Liu, H. and Gao, J., 2006. AVO inversion based on common shot migration. Appl. Geophys., 3: 98-104.

Shuey, R.T., 1985. A simplification of the Zoeppritz equations. Geophysics, 50: 609-614.

Sidler, R. and Holliger, K., 2010. Seismic reflectivity of the sediment-covered seafloor: effects of velocity gradients and fine-scale layering. Geophys. J. Internat., 181: 521-531.

Simmons Jr., J.L. and Backus, M.M., 1996. Waveform-based AVO inversion and AVO prediction-error. Geophysics, 61: 1575-1588.

Sun, X.P. and Zhao, L.W., 2006. Seismic Amplitude Interpretation (in Chinese). Petroleum Industry Press, Beijing.

Thomsen, L., 1986. Weak elastic anisotropy. Geophysics, 51: 1954-1966.

Tsvankin, I., 1995. Body-wave radiation patterns and AVO in transversely isotropic media. Geophysics, 60: 1409-1425.

Tura, A. and Lumey, D.E., 1999. Estimating pressure and saturation changes time-lapse AVO data. Expanded Abstr., 69th Ann. Internat. SEG Mtg., Houston: 1655-1658.

Vavryčuk, V., 1999. Weak-contrast reflection/transmission coefficients in weakly anisotropic elastic media: P-wave incidence. Geophys. J. Internat., 138: 553-562.

Wang, Y., 1999. Approximations to the Zoeppritz equations and their use in AVO analysis. Geophysics, 64: 1920-1927.

Zong, Z., Yin, X. and Wu, G., 2012. AVO inversion and poroelasticity with P-and S-wave moduli. Geophysics, 77(6), N17-N24.

APPENDIX A

The partial derivatives of matrix $\boldsymbol{A}$ with respect to η_1 are expressed as:

$$\frac{\partial A}{\partial \eta_1} = \frac{1}{\eta_1}\begin{pmatrix} 0 & -\sin\beta & 0 & 0 \\ 0 & -\tan\beta\sin\beta & 0 & 0 \\ -4\sin^2\beta & (\tan^2\beta - 2)\eta_1 \sin 2\beta & 0 & 0 \\ 2\eta_1^2 \sin 2\alpha & 3\eta_1 \cos 2\beta - 2\eta_1 & 0 & 0 \end{pmatrix}. \tag{A-1}$$

The partial derivatives of matrix $\boldsymbol{A}$ with respect to η_2 are given by:

$$\frac{\partial A}{\partial \eta_2} = \frac{1}{\eta_2}\begin{pmatrix} 0 & 0 & -\tan\alpha'\sin\alpha' & 0 \\ 0 & 0 & -\sin\alpha' & 0 \\ 0 & 0 & -\rho_{21}\eta_2 \cos 2\beta' & 0 \\ 0 & 0 & -\rho_{21}\dfrac{\eta_3^2}{\eta_2}\tan^2\alpha'\sin 2\alpha' & 0 \end{pmatrix}. \tag{A-2}$$

For η_3, the equations are expressed as:

$$\frac{\partial A}{\partial \eta_3} = \frac{1}{\eta_3}\begin{pmatrix} 0 & 0 & 0 & \sin\beta' \\ 0 & 0 & 0 & -\tan\beta'\sin\beta' \\ 0 & 0 & 2\rho_{21}\eta_2 - 2\rho_{21}\eta_2\cos 2\beta' & (\tan^2\beta' - 2)\rho_{21}\eta_3 \sin 2\beta' \\ 0 & 0 & 2\rho_{21}\dfrac{\eta_3^2}{\eta_2}\sin 2\alpha' & 2\rho_{21}\eta_3 - 3\rho_{21}\eta_3\cos 2\beta' \end{pmatrix}. \tag{A-3}$$

For a homogenous elastic medium, the P- and S-wave velocities are correlated with the density. Thus, the partial derivatives of η_1, η_2 and η_3 respect to the density ratio ρ_{21} can be obtained:

$$\frac{\partial \eta_1}{\partial \rho_{21}} = 0, \quad \frac{\partial \eta_2}{\partial \rho_{21}} = -\frac{1}{2\rho_{21}}\eta_2, \quad \frac{\partial \eta_3}{\partial \rho_{21}} = -\frac{1}{2\rho_{21}}\eta_3. \tag{A-4}$$

Based on the chain rule of derivation, we can combine the eq. (A-4) with eqs. (A-1)-(A-3) to derive the partial derivatives of matrix $\boldsymbol{A}$ with respect to ρ_{21} as:

$$\frac{\partial A}{\partial \rho_{21}} = \frac{1}{2\rho_{21}} \begin{pmatrix} 0 & 0 & \tan\alpha'\sin\alpha' & -\sin\beta' \\ 0 & 0 & \sin\alpha' & \tan\beta'\sin\beta' \\ 0 & 0 & \rho_{21}\eta_2\cos 2\beta' - 2\rho_{21}\eta_2 & -\rho_{21}\eta_3\tan^2\beta'\sin 2\beta' \\ 0 & 0 & \rho_{21}\dfrac{\eta_3^2}{\eta_2}\sin 2\alpha'\tan^2\alpha' & \rho_{21}\eta_3\cos 2\beta' - 2\rho_{21}\eta_3 \end{pmatrix} . \quad \text{(A-5)}$$

For matrix B, it can easily calculate the partial derivatives as:

$$\begin{cases} \dfrac{\partial B}{\partial \eta_1} = \dfrac{1}{\eta_1}\begin{pmatrix} 0 & 0 & -4\sin^2\beta & 2\eta_1^2\sin 2\alpha \end{pmatrix}^T \\ \dfrac{\partial B}{\partial \eta_2} = \dfrac{1}{\eta_2}\begin{pmatrix} 0 & 0 & 0 & 0 \end{pmatrix}^T \\ \dfrac{\partial B}{\partial \eta_3} = \dfrac{1}{\eta_3}\begin{pmatrix} 0 & 0 & 0 & 0 \end{pmatrix}^T \\ \dfrac{\partial B}{\partial \rho_{21}} = \dfrac{1}{2\rho_{21}}\begin{pmatrix} 0 & 0 & 0 & 0 \end{pmatrix}^T \end{cases} . \quad \text{(A-6)}$$

The derivatives of the SWRCs with respect to seismic wave velocities and medium density can be obtained by the chain rule for the ratios of the seismic wave velocities and the ratios of density.

$$\frac{\partial R_{PP}}{\partial V_{P1}} = \frac{\partial R_{PP}}{\partial \eta_2}\cdot\frac{\partial \eta_2}{\partial V_{P1}} = -\frac{V_{P2}}{V_{P1}^2}\frac{\partial R_{PP}}{\partial \eta_2}, \quad \frac{\partial R_{PP}}{\partial V_{P2}} = \frac{\partial R_{PP}}{\partial \eta_2}\cdot\frac{\partial \eta_2}{\partial V_{P2}} = \frac{1}{V_{P1}}\frac{\partial R_{PP}}{\partial \eta_2}. \quad \text{(A-7)}$$

$$\frac{\partial R_{PP}}{\partial V_{S1}} = \frac{\partial R_{PP}}{\partial \eta_1}\cdot\frac{\partial \eta_1}{\partial V_{S1}} = \frac{1}{V_{P1}}\frac{\partial R_{PP}}{\partial \eta_1}, \quad \frac{\partial R_{PP}}{\partial V_{S2}} = \frac{\partial R_{PP}}{\partial \eta_3}\cdot\frac{\partial \eta_3}{\partial V_{S2}} = \frac{1}{V_{P1}}\frac{\partial R_{PP}}{\partial \eta_3}. \quad \text{(A-8)}$$

$$\frac{\partial R_{PP}}{\partial \rho_1} = \frac{\partial R_{PP}}{\partial \rho_{21}}\cdot\frac{\partial \rho_{21}}{\partial \rho_1} = -\frac{\rho_2}{\rho_1^2}\frac{\partial R_{PP}}{\partial \rho_{21}}, \quad \frac{\partial R_{PP}}{\partial \rho_2} = \frac{\partial R_{PP}}{\partial \rho_{21}}\cdot\frac{\partial \rho_{21}}{\partial \rho_2} = \frac{1}{\rho_1}\frac{\partial R_{PP}}{\partial \rho_{21}}. \quad \text{(A-9)}$$

$$\frac{\partial R_{PS}}{\partial V_{P1}} = \frac{\partial R_{PS}}{\partial \eta_2}\cdot\frac{\partial \eta_2}{\partial V_{P1}} = -\frac{V_{P2}}{V_{P1}^2}\frac{\partial R_{PS}}{\partial \eta_2}, \quad \frac{\partial R_{PS}}{\partial V_{P2}} = \frac{\partial R_{PS}}{\partial \eta_2}\cdot\frac{\partial \eta_2}{\partial V_{P2}} = \frac{1}{V_{P1}}\frac{\partial R_{PS}}{\partial \eta_2}. \quad \text{(A-10)}$$

$$\frac{\partial R_{PS}}{\partial V_{S1}} = \frac{\partial R_{PS}}{\partial \eta_1}\cdot\frac{\partial \eta_1}{\partial V_{S1}} = \frac{1}{V_{P1}}\frac{\partial R_{PS}}{\partial \eta_1}, \quad \frac{\partial R_{PS}}{\partial V_{S2}} = \frac{\partial R_{PS}}{\partial \eta_3}\cdot\frac{\partial \eta_3}{\partial V_{S2}} = \frac{1}{V_{P1}}\frac{\partial R_{PS}}{\partial \eta_3}. \quad \text{(A-11)}$$

$$\frac{\partial R_{PS}}{\partial \rho_1} = \frac{\partial R_{PS}}{\partial \rho_{21}}\cdot\frac{\partial \rho_{21}}{\partial \rho_1} = -\frac{\rho_2}{\rho_1^2}\frac{\partial R_{PS}}{\partial \rho_{21}}, \quad \frac{\partial R_{PS}}{\partial \rho_2} = \frac{\partial R_{PS}}{\partial \rho_{21}}\cdot\frac{\partial \rho_{21}}{\partial \rho_2} = \frac{1}{\rho_1}\frac{\partial R_{PS}}{\partial \rho_{21}}. \quad \text{(A-12)}$$

APPENDIX B

The partial derivatives of the reflection coefficients with V_{P1}, V_{P2} and V_{S2}:

$$\begin{aligned}\frac{\partial R_{PS}^{anis}}{\partial V_{P1}} = \frac{\partial R_{PS}^{anis}}{\partial V_{P2}} = \frac{1}{2}\Bigg\{\Bigg[\Bigg(\frac{V_P}{(V_P^2-V_S^2)\cos\beta}-\frac{V_P^3}{(V_P^2-V_S^2)^2\cos\beta}\Bigg)\\ -\Bigg(\frac{V_S\cos\alpha}{2(V_P^2-V_S^2)}-\frac{V_P^2V_S\cos\alpha}{(V_P^2-V_S^2)^2}\Bigg)\Bigg](\delta_2-\delta_1)\sin\alpha\\ +\Bigg[\Bigg(\frac{V_S\cos\alpha}{(V_P^2-V_S^2)}-\frac{2V_P^2V_S\cos\alpha}{(V_P^2-V_S^2)^2}\Bigg)\Bigg](\delta_2-\delta_1+\varepsilon_1-\varepsilon_2)\sin^3\alpha\\ -\Bigg[\Bigg(\frac{2V_p}{(V_P^2-V_S^2)\cos\beta}-\frac{2V_P^3}{(V_P^2-V_S^2)^2\cos\beta}\Bigg)\Bigg](\delta_2-\delta_1+\varepsilon_1-\varepsilon_2)\sin^3\alpha\\ -\Bigg[\frac{V_pV_S^2}{(V_P^2-V_S^2)^2\cos\beta}\Bigg](\delta_2-\delta_1)\sin^3\alpha\\ -\Bigg[\frac{2V_pV_S^2}{(V_P^2-V_S^2)^2\cos\beta}\Bigg](\delta_2-\delta_1+\varepsilon_1-\varepsilon_2)\sin^5\alpha\Bigg\}\end{aligned} \quad . \qquad \text{(B-1)}$$

$$\begin{aligned}\frac{\partial R_{PS}^{anis}}{\partial V_{S2}} = \frac{1}{2}\Bigg\{\Bigg[\Bigg(\frac{V_P^2V_S}{(V_P^2-V_S^2)^2\cos\beta}\Bigg)-\Bigg(\frac{V_P\cos\alpha}{2(V_P^2-V_S^2)}-\frac{V_PV_S^2\cos\alpha}{(V_P^2-V_S^2)^2}\Bigg)\Bigg](\delta_2-\delta_1)\sin\alpha\\ +\Bigg[\Bigg(\frac{V_P\cos\alpha}{(V_P^2-V_S^2)}+\frac{2V_PV_S^2\cos\alpha}{(V_P^2-V_S^2)^2}\Bigg)\Bigg](\delta_2-\delta_1+\varepsilon_1-\varepsilon_2)\sin^3\alpha\\ -\Bigg[\frac{2V_P^2V_S}{(V_P^2-V_S^2)^2\cos\beta}\Bigg](\delta_2-\delta_1+\varepsilon_1-\varepsilon_2)\sin^3\alpha\\ +\Bigg[\Bigg(\frac{V_S}{(V_P^2-V_S^2)\cos\beta}+\frac{V_S^3}{(V_P^2-V_S^2)^2\cos\beta}\Bigg)\Bigg](\delta_2-\delta_1)\sin^3\alpha\\ +\Bigg[\Bigg(\frac{2V_S}{(V_P^2-V_S^2)\cos\beta}+\frac{2V_S^3}{(V_P^2-V_S^2)^2\cos\beta}\Bigg)\Bigg](\delta_2-\delta_1+\varepsilon_1-\varepsilon_2)\sin^5\alpha\Bigg\}\end{aligned} \qquad \text{(B-2)}$$

As we mentioned above, the $\cos\beta$ can be expressed as a function of V_{S1}. Therefore, we can get the partial derivative with V_{S1} as:

$$\begin{aligned}\frac{\partial R_{PS}^{anis}}{\partial V_{S1}} = \frac{1}{2}\Bigg\{&\Bigg[\Bigg(\frac{V_P^2 V_S}{(V_P^2-V_S^2)^2\cos\beta}-\frac{V_P^2\tan^2\beta}{2V_{S1}(V_P^2-V_S^2)\cos\beta}\Bigg)\\&-\Bigg(\frac{V_P\cos\alpha}{2(V_P^2-V_S^2)}-\frac{V_P V_S^2\cos\alpha}{(V_P^2-V_S^2)^2}\Bigg)\Bigg](\delta_2-\delta_1)\sin\alpha\\&+\Bigg[\Bigg(\frac{V_P\cos\alpha}{(V_P^2-V_S^2)}+\frac{2V_P V_S^2\cos\alpha}{(V_P^2-V_S^2)^2}\Bigg)\Bigg](\delta_2-\delta_1+\varepsilon_1-\varepsilon_2)\sin^3\alpha\\&-\Bigg[\Bigg(\frac{2V_P^2 V_S}{(V_P^2-V_S^2)^2\cos\beta}-\frac{2V_P^2\tan^2\beta}{V_{S1}(V_P^2-V_S^2)\cos\beta}\Bigg)\Bigg](\delta_2-\delta_1+\varepsilon_1-\varepsilon_2)\sin^3\alpha\\&+\Bigg[\Bigg(\frac{V_S}{(V_P^2-V_S^2)\cos\beta}+\frac{V_S^3}{(V_P^2-V_S^2)^2\cos\beta}\Bigg)\\&-\Bigg(\frac{V_S^2\tan^2\beta}{2V_{S1}(V_P^2-V_S^2)\cos\beta}\Bigg)\Bigg](\delta_2-\delta_1)\sin^3\alpha\\&+\Bigg[\Bigg(\frac{2V_S}{(V_P^2-V_S^2)\cos\beta}+\frac{2V_S^3}{(V_P^2-V_S^2)^2\cos\beta}\Bigg)\\&-\Bigg(\frac{V_S^2\tan^2\beta}{V_{S1}(V_P^2-V_S^2)\cos\beta}\Bigg)\Bigg](\delta_2-\delta_1+\varepsilon_1-\varepsilon_2)\sin^5\alpha\Bigg\}\end{aligned} \quad . \quad \text{(B-3)}$$

Then, we use the chain rule to generate the partial derivatives with respect to densities:

$$\begin{cases}\dfrac{\partial R_{PS}^{anis}}{\partial\rho_1} = \dfrac{\partial R_{PS}^{anis}}{\partial V_{P1}}\dfrac{\partial V_{P1}}{\partial\rho_1}+\dfrac{\partial R_{PS}^{anis}}{\partial V_{S1}}\dfrac{\partial V_{S1}}{\partial\rho_1}\\ \qquad = -\dfrac{V_{P1}}{2\rho_1}\dfrac{\partial R_{PS}^{anis}}{\partial V_{P1}}--\dfrac{V_{S1}}{2\rho_1}\dfrac{\partial R_{PS}^{anis}}{\partial V_{S1}}\\ \dfrac{\partial R_{PS}^{anis}}{\partial\rho_2} = \dfrac{\partial R_{PS}^{anis}}{\partial V_{P2}}\dfrac{\partial V_{P2}}{\partial\rho_2}+\dfrac{\partial R_{PS}^{anis}}{\partial V_{S2}}\dfrac{\partial V_{S2}}{\partial\rho_2}\\ \qquad = -\dfrac{V_{P2}}{2\rho_2}\dfrac{\partial R_{PS}^{anis}}{\partial V_{P2}}--\dfrac{V_{S2}}{2\rho_2}\dfrac{\partial R_{PS}^{anis}}{\partial V_{S2}}\end{cases} \quad . \quad \text{(B-4)}$$

Finally, we can easily compute the partial derivatives of the reflection coefficients with respect to Thomsen parameters ε and δ, respectively:

$$
\begin{cases}
\dfrac{\partial R_{PP}^{anis}}{\partial \delta_i} = \dfrac{(-1)^i}{2}\sin^2\alpha, \qquad \dfrac{\partial R_{PP}^{anis}}{\partial \varepsilon_i} = \dfrac{(-1)^i}{2}\sin^2\alpha\tan^2\alpha \\
\dfrac{\partial R_{Ps}^{anis}}{\partial \delta_i} = (-1)^i\left[\left(\dfrac{V_P^2}{2(V_P^2-V_S^2)\cos\beta} - \dfrac{V_PV_S\cos\alpha}{2(V_P^2-V_S^2)}\right)\sin\alpha\right] \\
\qquad\qquad +(-1)^i\left[\dfrac{V_PV_S\cos\alpha}{(V_P^2-V_S^2)}\right]\sin^3\alpha - (-1)^i\left[\dfrac{V_P^2}{(V_P^2-V_S^2)\cos\beta}\right]\sin^3\alpha \\
\qquad\qquad +(-1)^i\left[\dfrac{V_S^2}{2(V_P^2-V_S^2)\cos\beta}\right]\sin^3\alpha + (-1)^i\left[\dfrac{V_S^2}{(V_P^2-V_S^2)\cos\beta}\right]\sin^5\alpha \\
\dfrac{\partial R_{Ps}^{anis}}{\partial \varepsilon_i} = (-1)^{i+1}\left[\dfrac{V_PV_S\cos\alpha}{(V_P^2-V_S^2)}\right]\sin^3\alpha - (-1)^{i+1}\left[\dfrac{V_P^2}{(V_P^2-V_S^2)\cos\beta}\right]\sin^3\alpha \\
\qquad\qquad +(-1)^{i+1}\left[\dfrac{V_S^2}{(V_P^2-V_S^2)\cos\beta}\right]\sin^5\alpha
\end{cases}
\quad . \qquad \text{(B-5)}
$$